Fracture toughness behaviour of ferritic ductile cast iron

R. SALZBRENNER
Physical Metallurgy Division, 1832 Sandia National Laboratories, Albuquerque, New Mexico 87185, USA

The static rate fracture toughness of a series of eight heats of ductile cast iron has been measured. Samples from each heat were tested in a heat treated condition which produced a fully ferritic matrix. The dominant influence of carbide (primarily in a pearlitic form) in controlling the fracture toughness was thus eliminated in this study. The chemical composition and the microstructural feature size has also been measured directly from each specimen tested. A multiple linear regression method was used to establish a simple mathematical relationship between fracture toughness and the composition and microstructure. Fracture toughness was found to be strongly associated with the spacing (or size) of the graphite nodules in these fully ferritic ductile cast irons. Other features, including the composition, the ferrite grain size, or the amount of graphite (over the ranges examined), did not strongly influence the fracture toughness. Fracture toughness also did not correlate with tensile properties (i.e. strength or ductility) in these alloys. The results of this work can be used to develop an appropriate quality control program for applications which require assurance against fracture toughness related failures.

Nomenclature

YS	0.2% offset yield strength (MPa)
UTS	Ultimate tensile strength (MPa)
% El	% tensile elongation
% RA	% reduction in area
E	Young's modulus (MPa)
J_{Ic}	Elastic–plastic fracture toughness (from J-integral test) (kJ m^{-2})
K_{Ic}	Linear–elastic fracture toughness, (MPa m$^{1/2}$)
$V_v^{graphite}$	Volume fraction graphite
$d^{ferrite}$	Ferrite grain size
N_A	Nodule count on a random plane (number mm^{-2})
$\bar{D}_v$	Three-dimensional nodule diameter (mm)
$\bar{\lambda}_v$	Three-dimensional mean free nodule spacing (centre-to-centre) (mm)
$\bar{D}_A$	Average nodule diameter on a random plane ("two-dimensional size") (mm)
$\bar{\Lambda}_A$	Average nearest neighbour spacing (centre-to-centre) on a random plane ("two-dimensional spacing") (mm)
a to g	Constants in the multiple linear regression analysis

1. Introduction

Ductile cast irons are being used in an ever increasing variety of applications [1]. These applications generally attempt to take advantage of the enhanced ductility (when compared to conventional grey cast irons) which arises by controlling the shape of the graphite phase. Specific melting and casting techniques are used, which result in spherically shaped graphite as opposed to the flake shape found in grey cast irons [2]. Tensile strength and ductility can both be improved by the spheroidization process. A number of other studies have concentrated on developing an understanding of the tensile behaviour of ductile cast irons [3–9].

Recently, there have been efforts to use ductile cast iron in components for which fracture toughness is a concern (e.g. turbine casings, automotive components, transportation and storage casks for radioactive materials) [10]. Studies reported in the literature have demonstrated that a wide variation in fracture toughness is available in ductile cast irons [11–14]. Previous research has shown that the presence or absence of carbide in a pearlitic morphology surrounding the spherical graphite is the dominant feature which controls the fracture toughness [15–17]. The presence of pearlite in amounts of approximately 15% or more can cause the alloy to behave in a linear elastic manner (at even small thicknesses) with a fracture toughness in the range of 27 to 38 MPa m$^{1/2}$. In the relative absence of pearlite (say less than 10%, depending on its distribution in the matrix), ductile cast iron alloys generally behave in an elastic–plastic manner for thicknesses up to 12 inch or more, at temperatures significantly below -40° C. Most of the fracture toughness-related information which has been made available on low pearlite material has been reported as conditional linear elastic stress intensity values, i.e. so-called K_q numbers [12, 14, 18–21]. Such values are a dramatic underestimation of the true fracture toughness of these materials, and can be used for only the most overly conservative design analyses. Further, it is even

0022–2461/87 $03.00 + .12

unlikely that invalid linear elastic measurements will allow an accurate relative ranking of the fracture toughness of low pearlite alloys with respect to one another.

Elastic–plastic techniques, such as presented in the ASTM E-813 test for J_{Ic} [22], must be used to determine the fracture toughness of low pearlite ductile cast irons. The methodology for doing this has been previously described [15, 23]. The results of these fracture toughness measurements provide intrinsic materials property data which allow meaningful comparisons among various low pearlite alloys and as well, offer the opportunity to utilize these data in properly conservative design analyses. A limited amount of static rate J-integral fracture toughness information on ferritic ductile cast iron is available in the literature [15, 16, 24]. The results from these previous studies show room temperature toughness of ferritic ductile cast irons to be in the range of 60 to 90 MPa $m^{1/2}$ (where the results from elastic–plastic tests have been converted to linear elastic stress intensity values as described in [22]).

The evaluation of the toughness of elastic–plastic materials by measurement of crack opening displacement (COD) is generally favoured by British researchers. Holdsworth and Jolley [25–27] have applied the COD method to ferritic ductile irons. Their work demonstrated that the ductile-to-brittle transition temperature decreases with decreasing nodule spacing. The COD (at maximum load) in the ductile regime is directly proportional to the nodule spacing [26]. In measurement of the COD at crack initiation, however, they found the nodules to have no effect. In dealing with fracture toughness as measured by COD, there is no assurance that the critical COD values reported are independent of sample size. Also, there is no rigorous method of relating the fracture toughness results from J-integral testing with that from COD except under very restricted experimental conditions [28, 29]. Since there is no assurance that these conditions have been met, only a very qualitative comparison of the COD data with results of this work can be performed. This is considered in the discussion portion of this paper.

The current work was undertaken to establish a framework for understanding the causes of the large variation of the fracture toughness within different ductile cast irons that have low amounts of pearlite. Low pearlite ductile cast irons which exhibited variation in composition and microstructure were tested to obtain a valid measure of their fracture toughness. A linear regression analysis technique was used to establish a relationship between the toughness and the compositional and microstructural variations within these alloys. These results were compared to similar models [9], which relate the tensile behaviour to composition and microstructure. Understanding of the features which control the toughness of ductile cast irons will allow proper materials specifications to be written for those applications where toughness related failures must be prevented.

2. Experimental procedures

The tests reported in this study were conducted on several different ductile iron alloys. This section will describe the alloys used in this study, and their heat treatment along with the experimental methods which were used to establish the valid fracture toughness of each material. The methods which were used for microstructural and compositional identification will also be reported.

2.1. Material and composition

Eight test blocks of ductile cast irons were fabricated for this project by the Motor and Machinery Castings Company (Detroit, Michigan). Each test block had an original dimension of 45 cm width × 60 cm length × 20 cm depth and a mass of approximately 400 kg. The ingots were cast into a sand mould with a 7.5 cm iron chill plate on the bottom side only. The effect of the chill plate on one side only was to produce a block of material with a large change in microstructural feature size, ranging from relatively fine at the bottom, to coarse at the top. The samples tested in this study were taken from both the "fine" (i.e. bottom portion) and "coarse" (i.e. upper portion) microstructural segment of each ingot. Since a significant variation exists in the microstructure from ingot to ingot (and also from sample to sample within the same ingot), all microstructural measurements were conducted on metallographic samples extracted from each specimen. These measurements are detailed in following sections.

The ingots were cast to provide for a variation in amount of carbon, silicon and nickel such that their effect on mechanical properties could be determined. The chemical composition for each ingot was determined for most elements by emission spectroscopy and X-ray fluorescence. The exceptions were carbon and sulphur, which were measured by an infrared combustion analysis technique. The average base composition for the ingots is given in Table I, along with the different silicon, carbon, and nickel contents which (by design) varied appreciably from ingot to ingot.

Also tested in this study were samples from large commercial castings of ferritic ductile cast irons (made to the German GGG-40 specification). These samples were included in this study to demonstrate how actual high quality commercial ductile cast irons compare to the materials manufactured specifically for this study. The matrix of the commercial materials were 100% ferrite in the as-received condition, and thus heat treatment to eliminate pearlite was not required. The compositions of these materials are listed in Table I.

2.2. Heat treatment

The eight heats of material were delivered in the as-cast condition, with no heat treatment provided by the manufacturer. The as-cast material was examined, and each was found to contain up to 80% pearlite. The exact amount of pearlite however was found to vary from almost nil at the chilled end of some ingots, to the 80% value (in some compositions) near the slowly cooled (i.e. upper) portion. Since the presence of pearlite was found to be deleterious to both ductility and toughness behaviour [3, 9, 10, 15], a heat treatment was used [1, 30] to eliminate the carbide phase,

TABLE I Compositions of the ductile cast irons used in this study

Sample	Composition						
	C (wt %)	Si (wt %)	Ni (wt %)	S (wt %)	Cu (wt %)	Cr (wt %)	Mn (wt %)
1U	2.53	1.71	0.54	0.027	0.092	0.07	0.23
2U	2.82	1.64	0.66	0.018	0.085	0.08	0.25
3U	2.54	3.49	0.58	0.016	0.086	0.08	0.24
4U	2.96	1.75	0.97	0.027	0.088	0.08	0.24
5U	2.97	1.70	0.76	0.024	0.083	0.08	0.24
6U	2.56	3.20	0.95	0.013	0.091	0.08	0.24
7U	n.a.	n.a.	n.a.	n.a.	n.a.	n.a.	n.a.
8U	n.a.	n.a.	n.a.	n.a.	n.a.	n.a.	n.a.
1L	2.88	1.11	0.96	0.022	0.21	0.14	0.26
2L	2.83	1.07	1.08	0.024	0.20	0.13	0.25
3L	2.71	2.03	0.97	0.015	0.22	0.14	0.26
4L	3.06	1.16	1.42	0.022	0.21	0.14	0.23
5L	3.09	1.11	1.11	0.024	0.20	0.14	0.24
6L	2.69	1.96	1.32	0.013	0.20	0.14	0.25
7L	2.93	2.10	0.79	0.010	0.20	0.14	0.26
8L	2.91	2.07	0.94	0.007	0.21	0.14	0.25
"T"	3.60	1.91	0.03	0.006	0.05	0.07	0.24
"B"	3.10	1.60	0.36	0.004	0.06	0.03	0.20

and thus the pearlitic portions of the microstructure. This heat treatment involved heating the material to 900° C and holding for 4 h in order to dissolve the carbide phase into the (austenitic) matrix. The solutionizing (carbon decomposition) treatment was followed by a slow furnace cool (at about $10° C h^{-1}$) to 700° C, which allowed the carbon in the austenitic matrix to precipitate at the pre-existing graphite nodules. Increasing amounts of silicon, nickel, and carbon all tend to promote the graphitization process. The sample material was held at 700° C for 24 h to ensure a (nearly) complete graphitization. The cooling of the sample to room temperature was performed slowly to avoid the introduction of residual stresses. This procedure allowed essentially all the pearlite to be eliminated from those samples which underwent heat treatment (a maximum of 10% residual pearlite remained in some samples, but this highly spheroidized pearlite was found not to affect the fracture toughness). The heat treated materials in this study were thus a combination of essentially only two phases: ferrite and graphite.

2.3. Fracture toughness testing

Fracture toughness measurements were performed on compact tension specimens which were modified to allow measurement of the load line displacement required in *J*-integral testing. The compact tension specimens were 2.3 cm thick, and had a width of 5 cm. All of the specimens were side-grooved approximately 5.5% on each side (i.e. the net sample thickness was reduced to 2.0 cm) in order to keep the crack front straight during precracking and testing. All tests reported herein were conducted at quasi-static rates at room temperature. The test technique used a single specimen compliance unloading method which was previously calibrated against the multiple specimen method for ductile cast iron materials. A complete description of this test method appears in [15].

Standard tensile tests [31] were also performed on the alloys used in this study. The tensile tests were conducted at a rate of $0.003 cm sec^{-1}$, at room temperature. The 0.2% offset yield strength, *YS*, and the ultimate tensile strength, *UTS*, and the ductility as measured by the total elongation to failure, *% El*, and the total reduction in area, *% RA*, were determined for each alloy. Tensile samples were taken from locations corresponding to those from which the toughness specimens were taken.

2.4. Microstructural measurements

Sections of material were taken for metallographic (and compositional) analysis directly from tested fracture toughness specimens. This was done because of the rather large variations in microstructural feature size (and potentially composition) found within each ingot. Metallographic (and compositional) information was taken directly from the material actually tested, thus eliminating the possibility of incorrectly linking the test results with unrepresentative material.

Representative microstructures from the eight ingots cast for this study (including upper and lower sections of each casting) are shown in Fig. 1. The extremes of the range in nodule sizes found in these materials are shown. Fig. 1a shows the smallest nodule size, which was found in samples from the lower portion of Alloy 7. The largest nodule size was found in the upper portion of Alloy 4, which is shown in Fig. 1b. The nodules in most of the alloys were highly spherical in shape (i.e. Types I or II nodules [30] for a description of nodule types). The only exceptions to this were samples from the upper portions of Alloys 3 and 6, which contained large amounts of elongated (Type III) nodules. Fig. 1c is a micrograph from the upper portion of Alloy 3, which shows this non-spherical nodule formation. The microstructures of the two commercial ductile cast irons tested in this study are shown in Fig. 2. Their nodule sizes were intermediate in the range found in the Alloys (1 through 8) made for this study.

For this study, the microstructures were quantified by utilizing the procedures discussed in [32, 33]. Data were taken with an automated image analysis system (a Bausch and Lomb, Omnicon 3500) to determine the

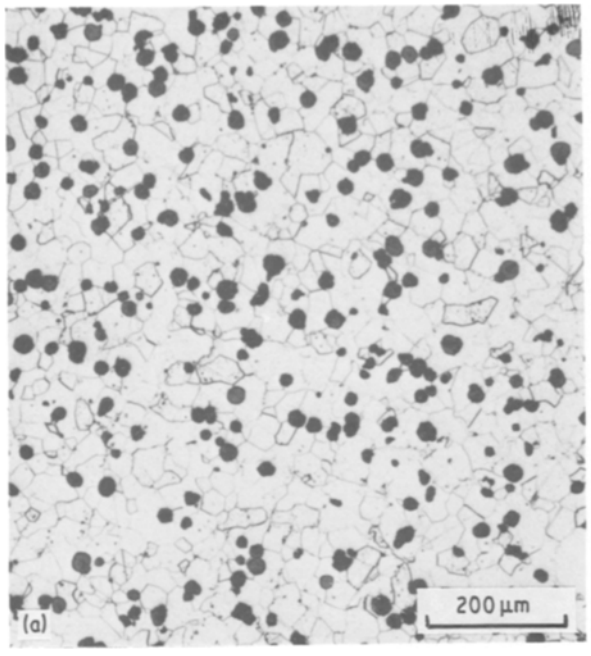

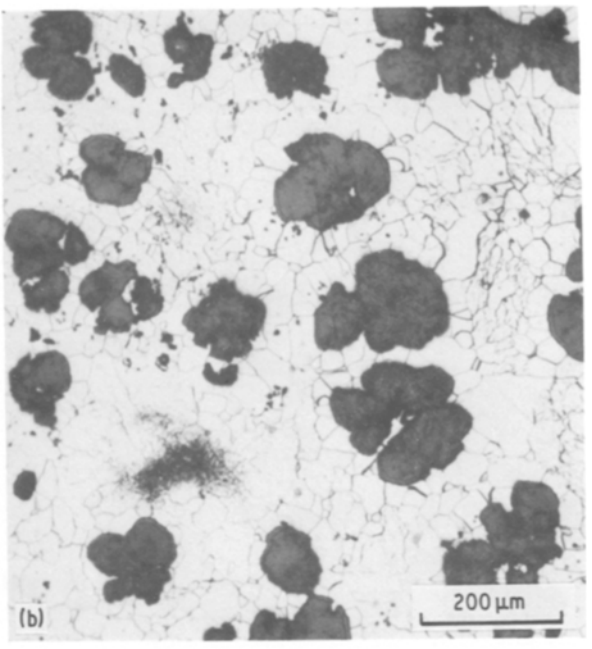

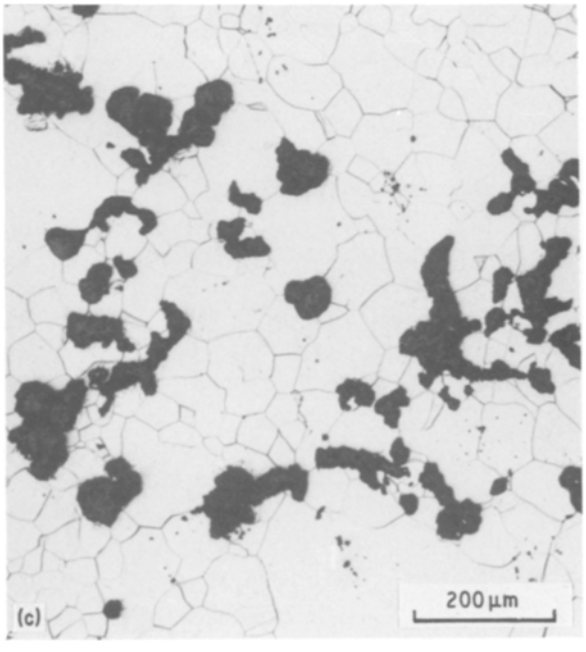

Figure 1 Optical micrographs show the extremes in the nodule size, spacing, and shape for the alloys tested in this study. (a) The smallest (spherical) nodule size and spacing was found in the lower (chilled) portion of Alloy 7. (b) The largest (approximately spherical) nodule size and spacing was found in the upper (slowly cooled) portion of Alloy 4. (c) Non-spherical nodules were observed in the upper portion of Alloy 3 (the upper portion of Alloy 6 had a similar microstructure).

actual (i.e. three-dimensional) nodule size distribution, by using a modified Scheil analysis. Although a normal distribution was found for several of the alloys (primarily those with the "fine" microstructure described earlier), a bimodal nodule size distribution has also measured in some of the alloys. Since a single normal distribution was not observed in all of the alloys, the standard deviation did not provide a meaningful parameter to compare with toughness variations. The mean nodule diameter, $\bar{D}_v$, was the only parameter used in this work to characterize the "3-D" nodule size. $\bar{D}_v$ was determined by summing the nodule diameters (after "correcting" the "2-D" observed distribution into the actual "3-D" nodule distribution) and dividing by the total number of nodules counted. The total number of nodules measured to determine the distribution was in the range of 500 to 5000.

A lineal intercept method was used to determine the mean free nodule (centre-to-centre) spacing, $\bar{\lambda}_v$, [32]. This spacing is the average distance between each particle and *all* of its neighbours. Linear intercept methods were also used to determine the ferrite grain size, d^{ferrite}, and the volume percentage of graphite nodules, V_v^{graphite}, present in each alloy. The number of intercepts measured in the determination of the above features, was in the range of 100 to 500.

The detailed determination of the three-dimensional distribution of graphite nodules in ductile cast irons is tedious; this is true even with the availability of automated image analysis equipment. As an alternative, a simplified manual method was employed to provide a straightforward method of quantitatively describing the changes in nodule distribution from sample to sample. These simplified measurements however do not contain all of the information necessary to uniquely define a particle distribution. Specifically, the simplified measurements do not provide direct information on the standard deviation or the number of particles per unit volume. Rather, these measurements provide a straightforward method of measuring the critical aspects of the nodule distribution as they relate to controlling the fracture toughness. The average 2-D graphite nodule diameter, $\bar{D}_A$, and spacing, $\bar{\Delta}_A$, were estimated from the graphite volume fraction (obtained from point count or linear intercept methods), and the nodule count. The nodule count (i.e. the number of nodules per unit area) is a technique which is commonly used to indicate the quality of ductile cast iron [30]. The values for $\bar{D}_A$ and $\bar{\Delta}_A$ were determined from counts of approximately 100 to 400 total nodules for each sample. Assuming that all of the nodules are

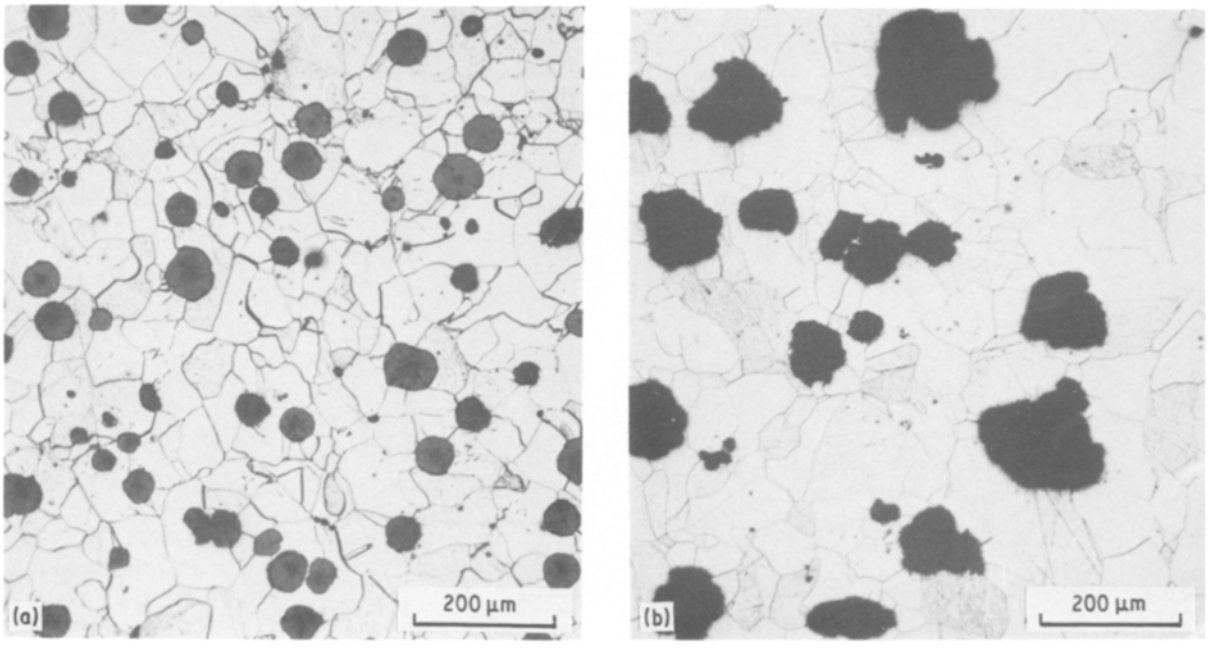

Figure 2 Optical micrographs show the microstructures of the two commercial ductile cast iron alloys tested in this work: (a) alloy "T", and (b) alloy "B".

circular in cross-section (i.e. spherical in three dimensions), the average nodule diameter can be calculated as:

$$\bar{D}_A = (4V_v^{graphite}/\pi N_A)^{1/2} \quad (1)$$

where $V_v^{graphite}$ is the volume fraction of graphite (from the lineal analysis), and N_A is the number of nodules mm^{-2} of material (on a random plane). A measure of the average centre-to-centre planar nodule spacing, $\bar{\Delta}_A$, can be determined as:

$$\bar{\Delta}_A = 0.5/(N_A^{1/2}) \quad (2)$$

This spacing is the average centre-to-centre distance between nearest neighbour particles. It is obvious that this determination of nodule spacing is not independent from the calculation of nodule diameter. All metallographic measurements (i.e. the three-dimensional and the simplified two-dimensional estimations) were directly compared, as shown in the following section.

TABLE II Mechanical properties of the ferritic ductile cast irons tested in this study

Sample	Fracture toughness J_{Ic} (kJ m^{-2})	Tensile properties			
		YS (MPa)	*UTS* (MPa)	% *El*	% *RA*
1U	73	250	360	7	11
2U	63	180	200	2	5
3U	52	390	410	2	2
4U	82	270	390	19	19
5U	75	190	240	7	8
6U	63	320	330	2	3
7U	79	390	480	15	14
8U	77	390	480	13	15
1L	45	250	390	20	28
2L	47	270	390	20	24
3L	25	340	440	7	8
4L	39	340	440	19	25
5L	39	270	380	18	26
6L	38	410	500	8	9
7L	21	430	530	15	23
8L	27	430	530	14	21
"T"	47	239	369	21	23
"B"	52	223	340	18	21

3. Results and discussion

3.1. Mechanical properties of heat treated alloys

The fracture toughness specimens were taken from both the lower, (more rapidly cooled) and the upper (more slowly cooled) portions of each ingot. The J_{Ic} fracture toughness values measured for all the samples tested in this program are reported in Table II. (The J_{Ic} values from these tests can be converted to equivalent K_{Ic} values as recommended in ASTM E 813 [22] by using the equation $K_{Ic} = (EJ_{Ic})^{1/2}$.) Also reported in Table II, are the average tensile properties from samples taken from the same region of each ingot. All of the alloys for which mechanical properties data are reported were heat treated to eliminate the embrittling (i.e. toughness reducing) effects of pearlite. The residual (highly decomposed) pearlite which remained after the heat treatment did not seem to have a major effect on the fracture toughness behaviour at room temperature.

As seen in Table II, there is a large range in the mechanical properties of the alloys measured in this program. In comparing the fracture toughness results with the tensile properties, there is no apparent correlation. For example, an alloy with a high ductility can exhibit either a high or low toughness (e.g. Samples 4U and 7L). Similarly, low tensile ductility can be present in high or low toughness alloys (e.g. Samples 6U and 3L). An examination of the strength–toughness combinations in these materials also leads to the conclusion that there is no strong relationship between these two properties.

3.2. Microstructural measurements

After the fracture toughness testing was completed,

TABLE III Microstructural features measured on the ductile cast irons used in this study

Sample	$V_v^{graphite}$ (%)	$d^{ferrite}$ (mm)	$\bar{D}_v$ (mm)	$\bar{\lambda}_v$ (mm)	N_A (number mm^{-2})	$\bar{D}_A$ (mm)	$\bar{\Delta}_A$ (mm)	$V_v^{pearlite}$ (%)	Nodule type
1U	11.4	0.071	0.167	0.755	19.9	0.085	0.118	< 5	100%-type II
2U	13.9	0.076	0.123	0.513	23.2	0.087	0.104	< 5	100%-type II
3U	13.8	0.057	0.134	0.299	71.3	0.050	0.059	0	60%-type II 40%-type III
4U	13.8	0.050	0.167	0.821	13.2	0.115	0.138	< 10	100%-type II
5U	10.2	0.057	0.136	0.808	13.0	0.100	0.139	< 10	100%-type II
6U	10.7	0.047	0.144	0.547	26.5	0.072	0.097	< 5	70%-type II 30%-type III
7U	13.0	0.050	n.a.	n.a.	17.7	0.097	0.119	0	100%-type II
8U	11.6	0.041	n.a.	n.a.	22.1	0.082	0.106	0	100%-type II
1L	12.7	0.029	0.078	0.287	75.1	0.046	0.058	0	90%-type I 10%-type II
2L	10.2	0.031	0.093	0.448	39.2	0.057	0.080	< 5	90%-type I 10%-type II
3L	14.7	0.032	0.052	0.148	176.2	0.033	0.038	0	90%-type I 10%-type II
4L	14.5	0.032	0.088	0.263	67.3	0.052	0.061	< 5	90%-type I 10%-type II
5L	13.0	0.029	0.075	0.246	99.3	0.041	0.050	0	90%-type I 10%-type II
6L	9.9	0.028	0.052	0.198	209.7	0.025	0.035	0	50%-type I 50%-type II
7L	8.9	0.026	0.031	0.159	353.2	0.018	0.027	0	90%-type I 10%-type II
8L	13.2	0.030	0.051	0.157	169.1	0.032	0.038	0	90%-type I 10%-type II
"T"	13.2	0.042	n.a.	n.a.	105.0	0.040	0.049	0	90%-type I 10%-type II
"B"	14.4	0.048	0.103	0.366	40.5	0.067	0.079	0	30%-type I 70%-type II

each specimen was sectioned to produce samples for chemical and microstructural analyses. These data are reported in Tables I and III.

The two-dimensional measurements of mean nodule size and spacing were found to be approximately linearly related to the three-dimensional determination of these features. This is shown graphically in Fig. 3. A linear relationship between $\bar{D}_v$ and $\bar{D}_A$ is expected, and should have the form:

$$\bar{D}_v = (\pi/2)\,\bar{D}_A \quad (3)$$

for spherically shaped particles [32]. The relationship between the "2-D" and "3-D" size measurements depends greatly on the nodule shape. As seen in Table III, almost all of the samples were composed primarily of Type I and II nodules which are highly spherical. The exceptions were samples from the upper portions of Alloys 3 and 6, which contained large amounts of non-spherical (Type III) nodules. The results from these two samples were not included in Fig. 3a, which is a plot of "2-D" against "3-D" diameters, and thus the linear relationship shown between the two methods of size measurements is limited to those materials which contain highly spherical nodules. As shown in Fig. 3a, the least squares straight line fit of the data provides a slope which is close to that theoretically predicted by Equation 3.

The measurement of the spacing between particles does not depend on any assumptions of nodule shape. As seen in Fig. 3b, there is a very good correlation (which includes results from samples 3U and 6U), between the two methods used in this study to characterize the nodule spacing. Fig. 3 verifies that since the different (i.e. the "2-D" and "3-D") techniques previously described, are linearly related, these methods measure essentially the same features (i.e. mean nodule size and spacing). Thus, it is appropriate to use the straightforward and easy "2-D" methods to quantify the mean nodule size and spacing.

3.3. Fracture toughness–microstructure–composition correlations

A convenient method of showing a relationship between properties (e.g. fracture toughness) and structure–composition, is to assume that a particular property is a dependent variable of the (assumed) independent variables of structure and composition. The simplest model for accomplishing this is a linear relationship between the dependent and independent variables. Thus, in such a model, the fracture toughness can be written as:

$$J_{Ic} = a + b(\%\ Ni) + c(\%\ Si) + d(\%\ C) + e(V_v^{graphite}) + f(L) + g(d^{ferrite}) \quad (4)$$

where a, b, c, d, e, f and g are constants. The term L, used in the equation above, stands for dimensions which represent the nodule distribution. Thus, L can be replaced in this equation in turn, by $\bar{\lambda}_v$, $\bar{\Delta}_A$, $\bar{D}_v$ or $\bar{D}_A$. % Ni, % Si and % C are the weight percentages of nickel, silicon and carbon, respectively. Because of the interrelationship between nodule size and spacing, values representing these quantities are not used simultaneously in the linear model shown in Equation 4.

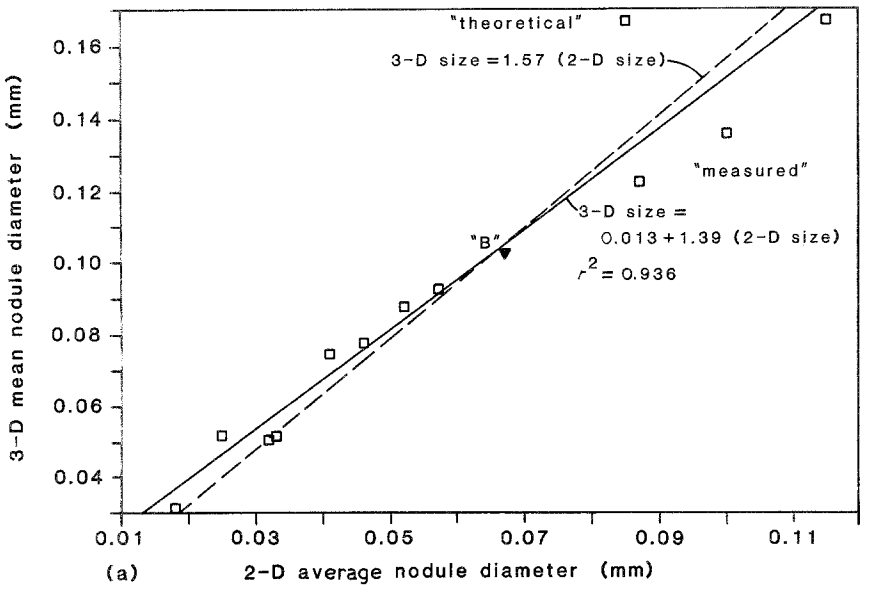

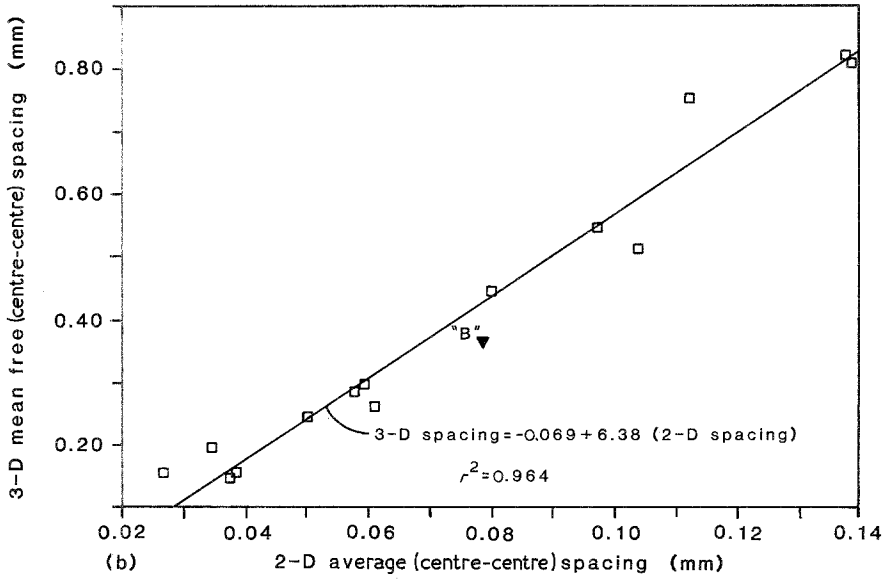

Figure 3 Comparison of the microstructural measurement methods used in this study: (a) average 3-D nodule diameter against average 2-D nodule diameter on a random plane, and (b) mean free (3-D) spacing between a nodule and all of its neighbours against average (2-D) spacing between nearest neighbour nodules on a random plane.

A multiple linear regression program*, was used to fit the data to the general model, by a process of minimizing the difference of squares [34]. It is clear however, that not all of the assumed independent variables have equal significance in a linear equation to predict the (dependent) fracture toughness. Thus the regression program was run in a stepwise fashion (both forward and backward) to either sequentially add in the most significant independent independent variables, or to eliminate the least significant variables from the linear model. The results from this iterative process produced a simple relationship between the fracture toughness and a measure of the nodule distribution as represented by $\bar{\lambda}_v$, $\bar{\Delta}_A$, $\bar{D}_v$ or $\bar{D}_A$. The other variables measured (i.e. ferrite grain size, volume fraction graphite, and composition) did not approach the significance of the nodule size or spacing in determining the overall fracture toughness of each alloy. The final model could thus be represented as:

$$J_{Ic} = a + f(L) \quad (5)$$

where the value used for L can be taken from the variables measured by the planar or volume methods described earlier. The values for the coefficients for each value of L are shown in Table IV. Also listed in the table are the parameters which detail the statistical significance of each model.

Figs 4 and 5 show measured values of fracture toughness against values predicted by equation. The equations used to determine Fig. 4 are based on the three-dimensional measurement of size and spacing. Those shown in Fig. 5 were established by using the simple planar (i.e. "2-D") microstructural measurements. The results of the regression analysis demonstrate that the fracture toughness is essentially independent of ferrite grain size, volume fraction graphite and composition (at least over the ranges measured). Since each linear equation for fracture toughness is dependent on a single parameter, values of that parameter can be linearly represented on the abscissa as shown on the upper part of each plot in Figs 4 and 5. This clearly depicts the dependence of the fracture toughness of ductile cast irons on the nodule spacing or size. Therefore if an appropriate measure of size or

*Run on a VAX 750, VMS 4.0 Version of SAS, SAS Institute Inc., Cary, North Carolina.

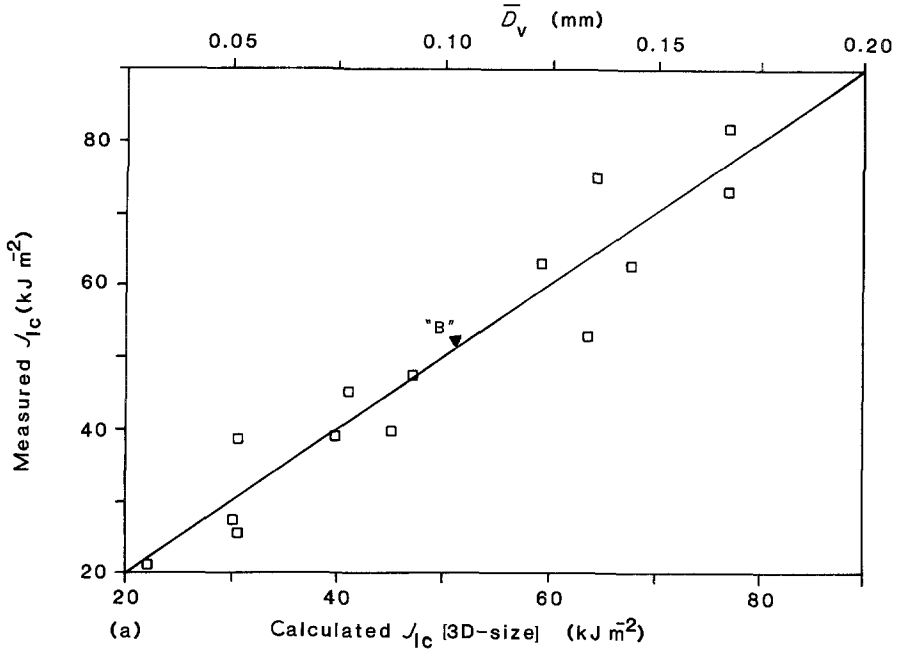

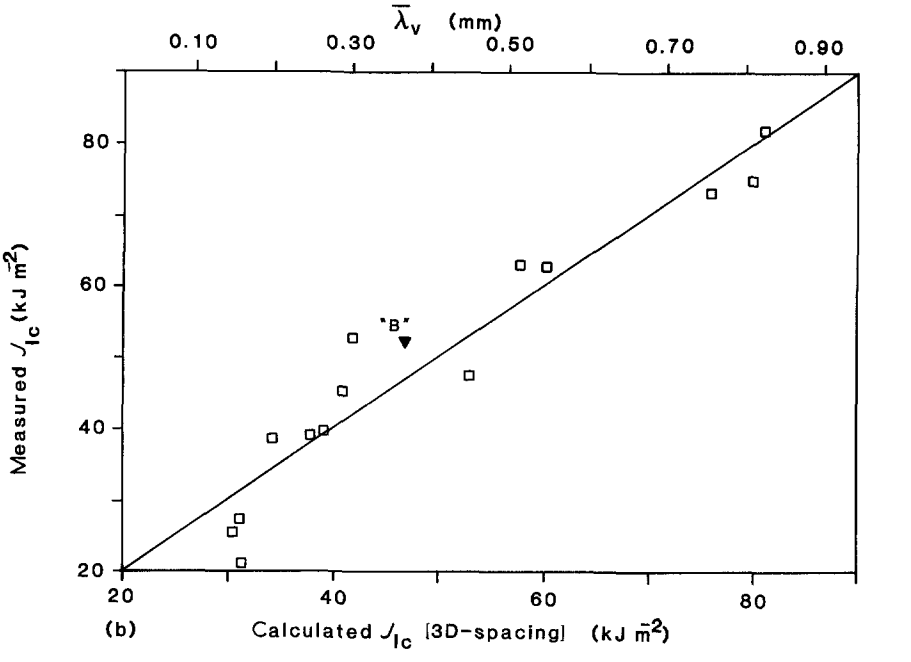

Figure 4 Measured values of initiation fracture toughness against values predicted by the linear regression model using: (a) average 3-D nodule size, and (b) mean free (3-D) nodule spacing. (a) $J_{Ic}^{calc} = 9.56 + 403\bar{D}_v$, $r^2 = 0.907$. (b) $J_{Ic}^{calc} = 19.4 + 74.8\bar{\lambda}_v$, $r^2 = 0.918$.

spacing is available, the toughness can be accurately estimated. These results further demonstrate that these nodule characteristics can be suitably measured on a plane, without transferring the results to the actual three-dimensional spatial relationships. The average (or mean) spacing or size alone seems to be an adequate measurement to estimate the fracture toughness to within approximately 20%. The distribution in nodule size or spacing within each sample has not been used in any of the models, and further, seems to be of secondary importance at most.

It is reasonable for the Mode I fracture toughness of ferritic ductile cast irons to be controlled by the planar microstructure, since this property is measured in a predominately planar fashion for these alloys. Specifically, the fracture during a test is constrained to a

TABLE IV Results of the stepwise multiple linear regression fit of the measured fracture toughness (as the dependent variable) with measured microstructural and compositional variables (as the independent variables)

Microstructural feature measured (mm)	Constant a (kJ m^{-2})	Coefficient f (kJ m^{-2} mm^{-1})	r^2	Standard error (kJ m^{-2})	F-test
$\bar{D}_v$	9.6	403	0.907	6.13	$F_{1,12} = 117$
$\bar{\lambda}_v$	19.4	74.8	0.918	5.75	$F_{1,12} = 134$
$\bar{D}_A$	12.4	659	0.907	6.46	$F_{1,14} = 136$
$\bar{\Delta}_A$	12.5	517	0.911	6.31	$F_{1,14} = 144$

The linear equation is of the form: $J_{Ic} = a + f(L)$, where $L = \bar{D}_v, \bar{\lambda}_v, \bar{D}_A$ or $\bar{\Delta}_A$. (For a 99% confidence level, $F_{1,12} > 9.33$ and $F_{1,14} > 8.86$).

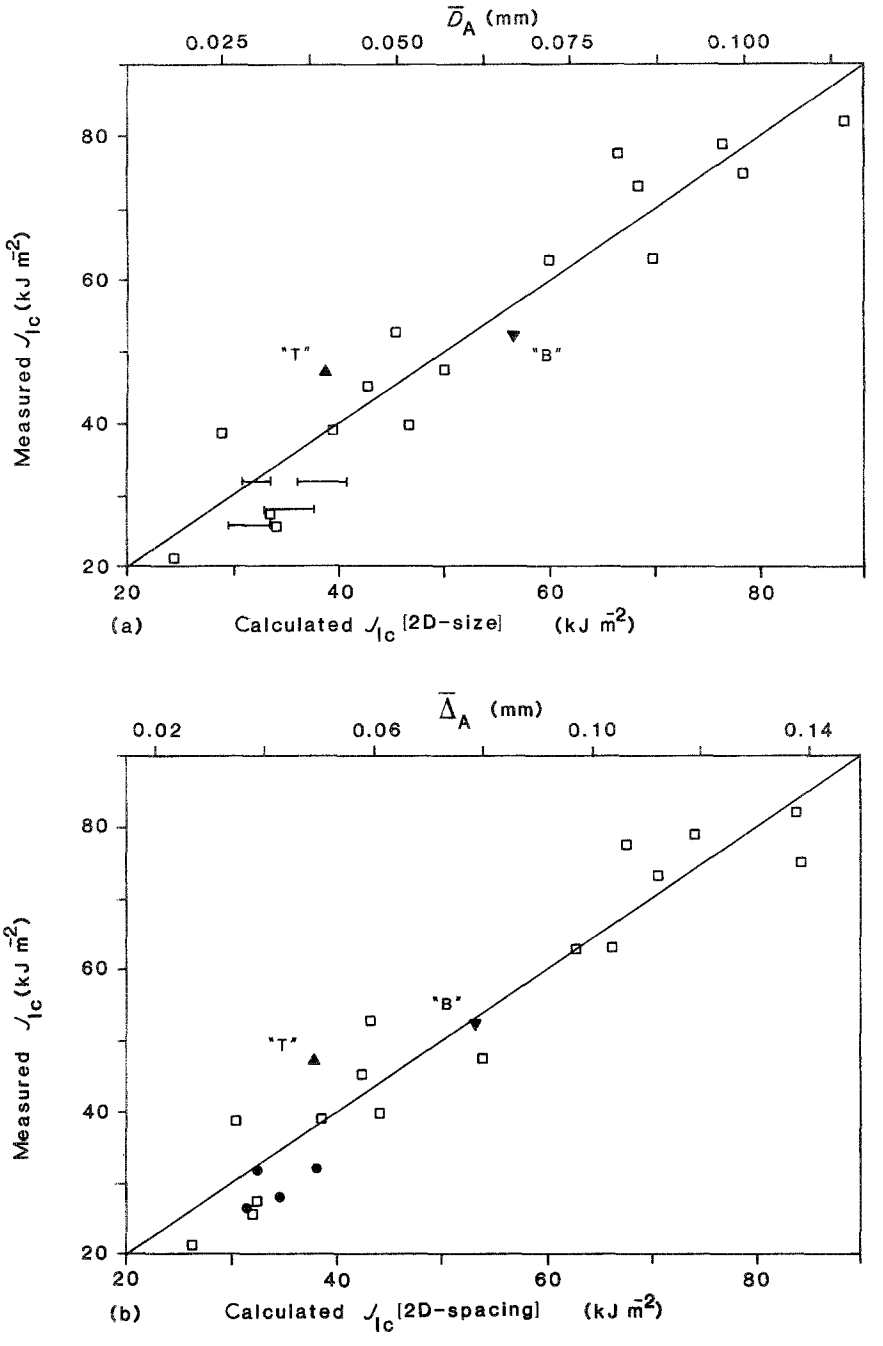

Figure 5 Measured values of initiation fracture toughness against values predicted by the linear regression model using; (a) average (2-D) nodule size on a random plane, and (b) average nearest neighbour nodule spacing on a random plane. (a) $J_{Ic}^{calc} = 12.4 + 659\bar{D}_A$, $r^2 = 0.907$. (⊢⊣) Estimated from data in [24]. (b) $J_{Ic}^{calc} = 12.5 + 517\bar{\Delta}_A$, $r^2 = 0.911$, (●) data from [24].

single, well-defined plane which is selected by the specimen-loading geometry. The planar nature of the cracking (through the centre of the test specimen) is shown by Fig. 6, which is an optical micrograph of a plane perpendicular to the crack plane containing the direction of crack growth. Thus for this special situation, the direct information contained in planar measurements may actually be preferred (over three-dimensional geometric relationships) for establishing structure/property relationships.

One important aspect of this research was the demonstration that a simplified (planar) measurement scheme for estimating particle size and spacing was appropriate for inclusion in a model which predicts fracture toughness. Such simplified measurement methods and techniques could be extremely useful for production quality control programs conducted at foundries producing large castings (e.g. nuclear transportation casks). Further, thick walled castings have a large gradation in microstructure from the edges to the centre, and thus it is important to determine what, if any, effect these microstructural changes have on properties such as fracture toughness.

As noted in several previous studies [10, 11, 15, 24, 27] the fracture of fully ferritic ductile cast irons (above the ductile-to-brittle transition temperature takes place by microvoid coalescence. Specific micromechanical models for this type of ductile fracture have been proposed [35–38]. These models show a dependency of initiation fracture toughness on the mean void-initiating particle spacing within the matrix. The data shown in Figs 4b and 5b supports the hypothesis that the graphite nodules act as void nucleation sites. Direct evidence of this is shown in Fig. 7, which is a scanning electron micrograph of the fracture surface (in the initiation region) typical of the alloys studied in this work.

The micromechanical models also include the dependency of the initiation toughness on the flow stress and a term which represents the critical strain at fracture.

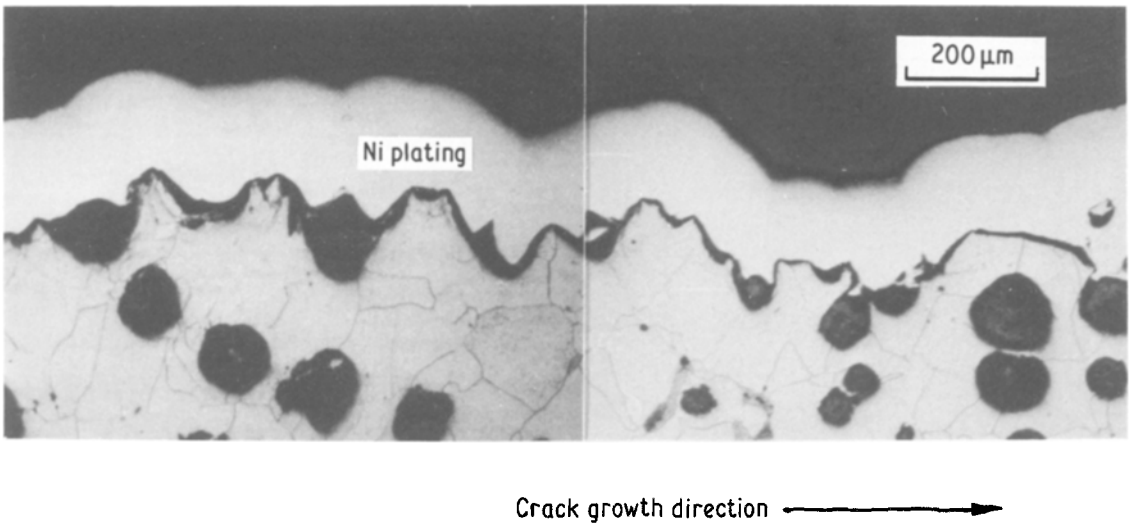

Figure 6 An optical micrograph showing the planar nature of the crack growth in the fracture toughness testing. The micrograph was taken on a plane through the centre of the specimen which was perpendicular to the crack plane.

This critical fracture strain is not simply related to conventionally measured tensile or plane strain ductilities, but is a function of the size, shape and spacing of void-initiating particles as well as the stress state. The evaluation of these terms is beyond the scope of the current paper, but the fact that J_{Ic} is (approximately) linearly related to nodule spacing, suggests that the product of the flow stress and critical fracture strain is approximately a constant for the set of materials tested.

3.4. Comparison with commercial alloys and previous studies

The equations generated in this study should be valid for all ductile cast irons which have nearly the same levels of impurities such as sulphur, phosphorus, etc.; these elements (particularly at higher levels) can dominate the fracture toughness behaviour. Thus, an alloy which has a significantly different content of these elements, may have a fracture toughness outside the range predicted by the equations derived in this work.

Fracture toughness of two other ferritic ductile cast irons were measured in this program (some data on material "T" were previously reported in [15]). These materials are representative of actual material cast into large castings (castings were 30 to 40 cm thick). The measured mechanical, compositional, and microstructural features are listed in Tables I through III. Values for fracture toughness were calculated by using the equations as listed in Table IV. These results are plotted on Figs 4 and 5. There is good agreement between the predicted and measured fracture toughness, and this suggests that the models generated for the ductile cast irons in this study can be reasonably

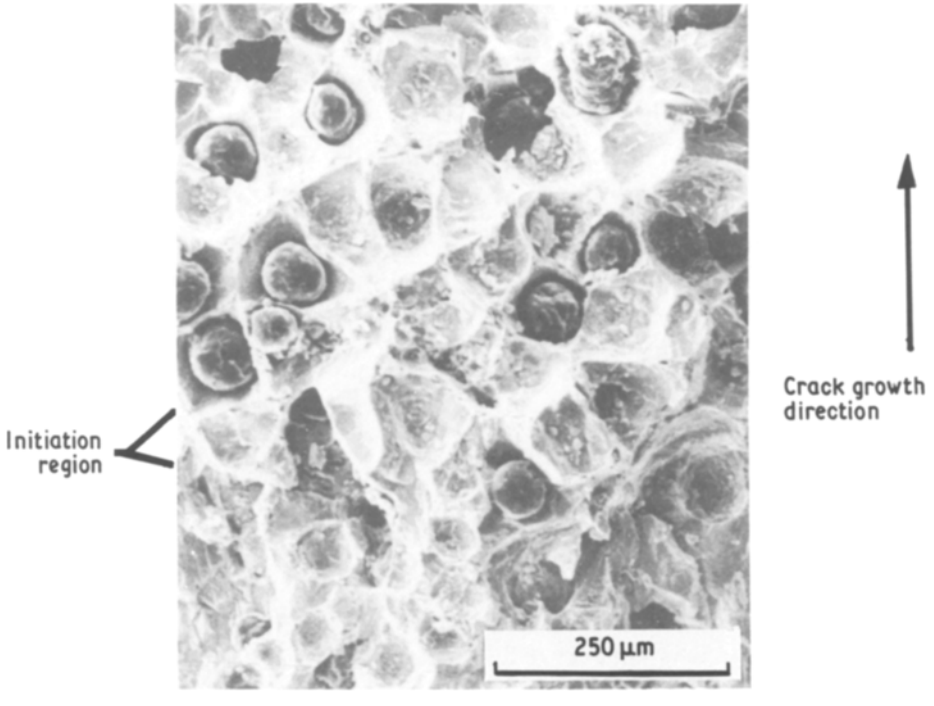

Figure 7 SEM micrograph of the initiation portion of the fracture surface displayed by ferritic ductile cast irons tested at room temperature. Nucleation occurs at the nodule/ferrite interface, and fracture occurs by microvoid coalescence.

TABLE V Fracture toughness and microstructural features for ductile cast iron samples tested by Le Douaron *et al.* [24]

Sample	Fracture toughness ($kJ\,m^{-2}$)	N_A (number mm^{-2})	$\bar{D}_A$* (mm)	$\bar{\Delta}_A$ (mm)
A	32	101	0.036–0.043	0.050
B	28	135	0.031–0.038	0.043
C	32	164	0.028–0.034	0.039
D	26	183	0.026–0.032	0.037

*Calculated by using Equation 1, and assuming $V_v^{graphite}$ is in the range of 10 to 15%.

applied to at least some commercially available (fully ferritic) materials.

Crack tip opening displacement (COD) measurement can (under rigorously controlled experimental conditions) provide a valid measure of the initiation fracture toughness of elastic–plastic materials. COD at initiation of crack extension was reported by Jolley and Holdsworth [27] for a number of fully ferritic ductile cast irons. They report that the initiation fracture toughness is independent of nodule size and spacing. This is in direct contrast to the results detailed earlier in this paper. Their conclusions also conflict with the direct evidence of the association between initiation and graphite nodules provided by scanning electron microscopy (see for example Fig. 7 and [10, 15, 24, 39]). Without further information concerning the exact experimental procedures used by Jolley and Holdsworth, a more detailed comparison of the actual initiation COD toughness values with the J_{Ic} numbers measured in this study is not possible. It should be noted however, that the range of nodule size and spacing for the alloys tested by Jolley and Holdsworth was smaller than that for the alloys considered in the present work. It is also important to note that their conclusions were based on a much smaller number of experiments than are presented in this paper.

A *J*-integral technique was employed by Le Douaron *et al.* [24] to measure the initiation fracture toughness of both as-cast and heat-treated ferritic ductile cast irons. Since nodule count measurements, as well as J_{Ic} values are presented in their paper, their results can be directly compared to the measurements presented in this paper. A summary of their data (for as-cast alloys) is presented in Table V, which includes "2-D" microstructural values calculated from their planar nodule count values. A range of "2-D" nodule diameters is presented which was based on assuming the volume percentage graphite was in the range of 10 to 15 vol %. The "2-D" microstructural data were further used in the relevant equations presented in Table IV, to calculate a predicted value for J_{Ic}. The comparison between predicted (i.e. calculated) values of toughness with those actually measured by Le Douaron *et al.* are shown in Fig. 5 (the range shown in Fig. 5a results from the assumption that the vol % graphite was 10 to 15%). There is satisfactory agreement of these values with the current work, especially considering errors that might be introduced from differences in technique used to measure toughness and microstructure. A further result reported by Le Douaron *et al.*, was that a ferritizing heat treatment resulted in the reduction of the fracture toughness of ductile cast irons. Such results were not seen in the current work, and it is especially clear (see Fig. 5) that proper heat treatment can bring the fracture toughness of ductile cast irons to levels equal to, or exceeding those of as-cast alloys.

3.5. Linear regression models for tensile properties

The relationship between tensile properties and the microstructure and composition for the alloys described in this study was previously reported [9]. The stepwise regression solution for the yield strength and for the ultimate tensile strength demonstrated that these properties are primarily dependent on the alloy composition of the matrix. Further, these strength properties are effectively independent of the microstructural features (at least over the range present in the alloys used in this study). The linear equation for strength (either yield or ultimate) is:

$$\text{strength} = a + b(\%\ Ni) + c(\%\ Si) \quad (6)$$

where the constants for a, b and c are listed in Table VI. This equation shows the effectiveness of silicon and nickel as solid solution strengtheners in these alloys. Carbon does not strongly affect the strength since the heat treatment causes the carbon to precipitate as graphite at the pre-existing nodules.

A suitable linear model relating the tensile ductility to the compositional and microstructural features measured could not be obtained for these alloys. This result indicated that a more complicated model (either in terms of compositional and microstructural features not measured, or in non-linear interaction of each independent microstructural and compositional variable) must be used to describe the tensile ductility.

These results thus show that fracture toughness, tensile strength and tensile ductility are each controlled by different variables. Fracture toughness is governed by the nodule distribution. Strength is determined almost entirely by composition. Ductility on the other hand, did not bear a simple relationship to the parameters measured. It is nonetheless clear that each of

TABLE VI Results of the stepwise multiple linear regression fit of the measured strength from tensile tests (as the dependent variable) with measured microstructural and compositional variables (as the independent variables)

Property	Linear model			Statistical fit parameters		
	Constant a (MPa)	Coefficient b (MPa/% *Ni*)	Coefficient c (MPa/% *Si*)	r^2	Standard error (MPa)	F-test ($F_{2,12}$)
YS	135	118	105	0.958	17.6	137
UTS	286	85.6	84.6	0.898	22.9	59.2

The linear equation is of the form: strength $= a + b(\%\ Ni) + c(\%\ Si)$. (For a 99% confidence level, $F_{2,12} > 6.93$).

these mechanical properties are not directly coupled. There is not a simple tradeoff between strength, ductility and toughness for fully ferritic ductile cast irons. This then suggests that there is the opportunity to optimize the composition and microstructure in order to obtain the best combination of mechanical properties for a particular application. An important auxiliary result that should be apparent, is that the acceptability of a particular material for a fracture sensitive design cannot be gained solely from tensile test results. For such applications, the fracture toughness must be monitored directly either via actual fracture toughness testing, or by measurement of specific features (such as nodule spacing) which have previously been shown to correlate with fracture toughness for the materials of interest.

4. Summary and conclusions

This investigation has examined the fracture toughness from eight heats of ductile cast iron. This study has shown that:

1. Fracture toughness can be validly determined with a J-integral method for a wide range of fully ferritic ductile cast irons.
2. The microstructural features in ductile cast iron which control the toughness can be appropriately measured by using simple two-dimensional techniques.
3. A linear relationship can be used to associate the fracture toughness of fully ferritic ductile irons to the size and spacing (based on either a "2-D" or "3-D" measurement scheme) of the graphite nodules present in each alloy.
4. The linear regression model for toughness was shown to be significantly different from those previously described for tensile strength and ductility for these same alloys.
5. Since the regression analyses has shown that fracture toughness, strength and ductility are essentially de-coupled for ductile cast irons, ductile cast iron alloys might be designed with particular combinations of microstructure and composition to produce optimized alloys for specific applications.
6. Since fracture toughness has been fundamentally shown to be effectively independent of tensile properties, fracture toughness cannot in general be predicted from tensile data for ferritic ductile cast irons.

Acknowledgements

I would like to thank Thomas B. Crenshaw for his able efforts in the fracture toughness testing portion of this research. I am also grateful to my colleagues at Sandia for their helpful discussions and suggestions. This work was performed at Sandia National Laboratories supported by the US Department of Energy under contract number DE-AC04-76DP00789.

References

1. "Metals Handbook", 9th edn Vol. 1 "Properties and Selection: Iron and Steels" (American Society for Metals, Metals Park, Ohio, 1978) pp. 33–56.
2. C. F. WALTON and T. J. OPAR (eds) "Iron Castings Handbook" (Iron Castings Society, Inc., 1981) p. 121.
3. A. H. RAUCH, J. B. PECK and E. M. McCULLOUGH, *AFS Transactions* **67** (1959) 111.
4. J. PELLEG, *Modern Castings* **43** (1963) 108.
5. G. J. COX, *Foundry Trade Journal* **28** (1974) 741.
6. O. YANAGISAWA and T. S. LUI, *Metallurgical Transactions A* **16A** (1985) 667.
7. H. FLEMMING and O. LIESENBERG, *Freiberg. Forschungsh. B* **178** (1975) 73.
8. A. FONTAINE and G. ZAMBELLI, *J. Mater. Sci.* **20** (1985) 4139.
9. R. SALZBRENNER, *Sandia Report*, SAND 86-0470 (Sandia National Laboratories, Albuquerque, New Mexico, 1985).
10. W. L. BRADLEY, *J. Metals* **37**(1) (1985) 74.
11. N. LAZARDIS, R. K. NANSTAD, F. J. WORZALA and C. R. LOPER Jr, *Amer. Found. Soc. Trans.* **85** (1977) 277.
12. R. K. NANSTAD, F. J. WORZALA and C. R. LOPER Jr, *Amer. Found. Soc. Trans.* **83** (1975) 245.
13. E. HORNBOGEN, *J. Mater. Sci.* **20** (1985) 3897.
14. B. OSTENSSON, *Scand. J. Metallurgy* **2** (1973) 194.
15. R. SALZBRENNER, J. A. VAN DEN AVYLE, T. J. LUTZ and W. L. BRADLEY, Proceedings of the Sixteenth Symposium on Fracture Mechanics, ASTM STP 868, edited by M. F. Kanninen and A. T. Hopper (American Society for Testing and Materials, Philadelphia, 1985) pp. 328–44.
16. W. L. BRADLEY and H. E. MEAD Jr, Proceedings of AFS 84th Annual Meeting (American Foundation Society, Des Plaines, 1980) pp. 126.
17. J. HWANG, J. DOONG and H. CHEN, *J. Mater. Sci. Lett.* **2** (1983) 737.
18. F. J. WORZALA, R. W. HEINE and Y. W. CHENG, *Amer. Found. Soc. Trans.* **82** (1976) 675.
19. F. J. WORZALA, R. K. NANSTAD and C. R. LOPER Jr, Proceedings of 5th Conference on Dimensioning and Calculations, Budapest, 1974, pp. 265–276.
20. H. J. SHETH and M. P. DIXIT, *Metall. Eng.* **10** (1979) 18.
21. J. MOTZ, D. BERGER, G. COHRY, G. KUHN, H. REUTER, D. SCHOCK, W. SHAKESHAFT and D. WOLTERS, *Giessereiforschung* **32** (1980) 97.
22. ASTM E-813, "Annual Book of ASTM Standards, Part 10, Metals Physical, Mechanical, Corrosion Testing" (American Society for Testing and Materials, Philadelphia, 1981) pp. 810–828.
23. J. A. JOYCE and J. P. GUDAS, "Elastic–Plastic Fracture, ASTM STP 668", edited by J. D. Landes, J. A. Begley and G. A. Clark (American Society for Testing and Materials, Philadelphia, 1979) pp. 451–468.
24. A. Le DOUARON, R. LAFONT, D. POULAIN and C. CLOITRE, *AFR* **1** (1978) 255.
25. S. R. HOLDSWORTH and G. JOLLEY, *British Foundrymen* **67** (1974) 77.
26. *Idem*, in Proceedings of the Second International Symposium on the Metallurgy of Cast Iron, edited by B. Lux, I. Minkoff and F. Mollard, Geneva, 1974, (sponsored by Battelle Geneva Research Centre, Geneva, Switzerland) pp. 809–825.
27. G. JOLLEY and S. R. HOLDSWORTH, "Fracture 1977" (University of Waterloo, Waterloo, Ontario, Canada, 1977) Vol. 12, pp. 403–13.
28. G. G. CHELL and I. MILNE, "Elastic–Plastic Fracture", Vol. II: Fracture Resistance Curves and Engineering Applications, ASTM STP 803, edited by C. F. Shih and J. P. Gudas (American Society for Testing and Materials, Philadelphia, 1981) pp. 179–205.
29. Y. XIAO and G. HUANG, *Eng Fracture Mech.* **16**(1) (1984) 83.
30. S. I. KARSAY, "Ductile Iron Production Practices" (American Foundation Society, Des Plaines, 1975) p. 148.
31. ASTM E-8, Annual Book of ASTM Standards, Part 10, Metals Physical, Mechanical, Corrosion Testing (American Society for Testing and Materials, Philadelphia, 1981) pp. 197–216.
32. E. E. UNDERWOOD, "Quantitative Microscopy", edited by R. T. DeHoff and F. N. Rhines (McGraw-Hill, New York, 1968) pp. 151–200.
33. H. J. RACK and R. W. NEWMAN, in "Physical Metallurgy", edited by R. W. Cahn (North-Holland, London,

1970) pp. 705–86.
34. P. R. BEVINGTON, "Data Reduction and Error Analysis for the Physical Sciences" (McGraw-Hill, New York, 1969).
35. J. R. RICE and D. M. TRACEY, *J. Mech. Phys. Solids* **217** (1969) 201.
36. R. O. RITCHIE, W. L. SERVER and R. A. WULLAERT, *Metall. Trans. A* **10A** (1979) 1557.
37. R. C. BATES, in "Metallurgical Treatises", edited by J. K. Tien and J. F. Elliott (The Metallurgical Society of AIME, Warrendale, 1982) pp. 551–70.
38. R. O. RITCHIE and A. W. THOMPSON, *Metall. Trans. A* **16A** (1985) 233.
39. P. J. PICKARDS, *J. Iron and Steel Institute* **193** (1971) 190.

Received 29 July
and accepted 22 September 1986